PLIN5 deficiency ameliorates metabolic dysfunction-associated fatty liver disease by inhibiting ferroptosis

YA LI[1,2*], XIAOHAN WANG[3*], XUECUI YIN[2,4*], XIAOHUI ZHU[3], WEIQI CUI[5], LIN DONG[3], YU XIA[3], YING WANG[6], LIU LIU[3], PENGYUAN ZHENG[4] and YOUCAI TANG[1,3]

[1]Henan Joint International Research Laboratory of Chronic Liver Injury and Henan Provincial Outstanding Overseas Scientists Chronic Liver Injury Workshop, Henan Key Laboratory of Rehabilitation Medicine, The Fifth Affiliated Hospital of Zhengzhou University, Zhengzhou, Henan 450000, P.R. China; [2]Henan Key Laboratory of *Helicobacter pylori*, Microbiota and Gastrointestinal Cancer, Marshall Medical Research Center, The Fifth Affiliated Hospital of Zhengzhou University, Zhengzhou, Henan 450000, P.R. China; [3]Department of Pediatrics, The Fifth Affiliated Hospital of Zhengzhou University, Zhengzhou, Henan 450000, P.R. China; [4]Department of Gastroenterology, The Fifth Affiliated Hospital of Zhengzhou University, Zhengzhou, Henan 450000, P.R. China; [5]Department of Pharmacy, The Fifth Affiliated Hospital of Zhengzhou University, Zhengzhou, Henan 450000, P.R. China; [6]Department of Blood Transfusion, The Fifth Affiliated Hospital of Zhengzhou University, Zhengzhou, Henan 450000, P.R. China

Received June 5, 2025; Accepted September 3, 2025

DOI: 10.3892/mmr.2025.13714

Abstract. Metabolic-associated fatty liver disease (MAFLD) is widely recognized as the most common type of chronic liver disease. As a member of the perilipin (PLIN) family, PLIN5 serves an important role in the regulation of lipid metabolism. Ferroptosis is a form of iron-dependent non-apoptotic cell death characterized by lipid peroxidation. Notably, knockout of *PLIN5* can attenuate high-fat diet (HFD)-induced MAFLD; however, the specific underlying mechanism remains unclear. The present study induced *PLIN5* overexpression by transfecting AML12 cells with a pcDNA3.1-*PLIN5* plasmid, and *PLIN5* knockdown was achieved using short hairpin RNA-mediated interference. Subsequently, intracellular ferrous iron (Fe^{2+}) levels were assessed via immunofluorescence staining. Furthermore, a MAFLD model was established in C57BL/6J mice by feeding them a HFD. To establish an *in vitro* model of hepatic steatosis, AML12 hepatocytes were treated with palmitic acid and oleic acid to induce intracellular lipid accumulation. To further explore the effects of PLIN5 on ferroptosis, liver single-cell sequencing was conducted and cellular experiments were performed to assess changes in redox and ferroptosis-related proteins. The current study investigated the effects of PLIN5 on MAFLD in animal and cellular experiments, including the changes in lipid accumulation, redox and ferroptosis-related markers. The results revealed that genetic knockdown of *PLIN5* significantly attenuated lipid accumulation and intracellular Fe^{2+} levels in AML12 hepatocytes, whereas *PLIN5* overexpression markedly exacerbated these parameters. In addition, *PLIN5* deficiency substantially reduced malondialdehyde content while enhancing glutathione levels, indicating attenuated oxidative stress. The results of the *in vivo* studies demonstrated that *PLIN5* knockout effectively ameliorated MAFLD progression in mice by suppressing ferroptosis. In conclusion, *PLIN5* knockout may delay the progression of MAFLD in mice via ferroptosis inhibition. Therefore, targeting PLIN5 could offer a novel therapeutic strategy to address MAFLD by modulating lipid metabolism and ferroptosis pathways.

Correspondence to: Professor Youcai Tang, Henan Joint International Research Laboratory of Chronic Liver Injury and Henan Provincial Outstanding Overseas Scientists Chronic Liver Injury Workshop, Henan Key Laboratory of Rehabilitation Medicine, The Fifth Affiliated Hospital of Zhengzhou University, 3 Kangfuqian Street, Zhengzhou, Henan 450000, P.R. China
E-mail: tangyoucai@hotmail.com

Professor Pengyuan Zheng, Department of Gastroenterology, The Fifth Affiliated Hospital of Zhengzhou University, 3 Kangfuqian Street, Zhengzhou, Henan 450000, P.R. China
E-mail: pyzheng@zzu.edu.cn

*Contributed equally

Key words: perilipin 5, metabolic-associated fatty liver disease, activating transcription factor 3, ferroptosis, lipid accumulation

Introduction

Metabolic-associated fatty liver disease (MAFLD) is newly approved nomenclature intended to expand the diagnostic criteria and avoid the stigma associated with the condition previously known as non-alcoholic fatty liver disease (NAFLD). This condition includes a range of liver conditions, from simple fatty liver (hepatic steatosis), which can be detected using imaging or histological methods, to metabolic-associated steatohepatitis (MASH), which is associated with inflammation and can result in more severe liver damage (1-3). The development of MAFLD is related to lipid accumulation, lipotoxicity, oxidative stress and endoplasmic

reticulum stress (ERS) (4), and the mechanism is complex. The US Food and Drug Administration approved resmetirom as a therapeutic drug for MASH in March 2024 (5), marking a major breakthrough in the treatment of MASH. However, the mechanism of MAFLD needs to be further explored to lay the foundation for developing more effective treatment strategies and preventive measures for MAFLD.

The excessive accumulation of lipid droplets (LDs) is a specific characteristic of MAFLD. Triglycerides (TGs) accumulate in hepatic LDs, which regulate intracellular fatty acid flux by storing and releasing fatty acids for oxidation or re-esterification into TGs or other complex lipids, thus preventing cytotoxic events (6,7). Perilipin (PLIN)5 is a member of the PLIN protein family, which has been reported to be positively associated with TG storage, fatty acid oxidation, lipotoxicity and metabolic dysfunction (8). PLIN5 is predominantly expressed in tissues with high oxidative metabolism, such as the liver, heart, skeletal muscle and brown adipose tissue (BAT) (9). The absence of PLIN5 can protect against liver injury in MAFLD by reducing inflammasome activation (10). Furthermore, our previous studies have shown that knockout of *PLIN5* can attenuate high-fat diet (HFD)-induced MAFLD in mice (11,12); however, its underlying molecular mechanism remains unclear.

Ferroptosis is a form of iron-dependent, non-apoptotic cell death characterized by lipid peroxidation. This unique mode of cell death is regulated by several cellular metabolic pathways, including iron metabolism and ERS, as well as various disease-related signaling pathways, such as glucose-regulated AMPK signaling (13). Notably, ferroptosis has gained attention in the field of liver disease as the liver is susceptible to oxidative damage, and excessive iron accumulation is a major feature in most primary liver diseases (14). Iron overload accelerates the dysfunction of lipid metabolism and liver injury in MAFLD, and inhibition of ferroptosis can be used to prevent and protect against various chronic liver injuries caused by iron deposition and abnormal lipid metabolism (15). MAFLD alters iron metabolism in the body and MAFLD progression is accompanied by extensive lipid accumulation (16-18). Therefore, ferroptosis is considered an emerging strategy in MAFLD therapeutics.

Activating transcription factor 3 (ATF3) belongs to the ATF/cAMP response element-binding (CREB) transcription factor protein family, which controls the expression of target genes by attaching to the specific DNA sequence TGACGTCA (19). ATF3 sensitizes gastric cancer cells to cisplatin through the induction of ferroptosis by blocking Nrf2/Keap1/xCT signaling (19). In addition, it has been shown that ATF3 has the ability to suppress the transcriptional activity of *SLC7A11*, a crucial gene involved in ferroptosis, thereby triggering the process of ferroptosis (20). Furthermore, ATF3-dependent induction of RIPK3 causes a modal shift in hepatocellular death from apoptosis to necroptosis, and has an important role in MASH (21). Therefore, it could be hypothesized that ATF3 may participate in the regulation of ferroptosis in MAFLD.

This present study aimed to investigate the involvement of PLIN5 in MAFLD progression and to determine if its role is related to ferroptosis. Comprehensive experiments were conducted to elucidate the underlying molecular mechanisms using both cellular and animal models.

Materials and methods

Animal models. A total of 20 C57BL/6J mice were obtained from Beijing Huafukang Biotechnology Co., Ltd. In addition, 20 *PLIN5*$^{-/-}$ mice were generated at the Nanjing Biomedical Research Institute of Nanjing University (Nanjing, China) and were identified via gene expression. *PLIN5*$^{-/-}$ mice were generated using a CRISPR/Cas9 system in the C57BL/6 background. *In vitro* transcribed guide RNA (gRNA) was co-injected with Cas9 protein into mouse fertilized eggs. Guided by the gRNA, the Cas9 protein binds to the target genomic site and induces double-strand breaks. These breaks are subsequently repaired via non-homologous end joining, leading to deletion mutations and ultimately resulting in gene knockout. Four single gRNAs (sgRNA1, sgRNA2, sgRNA3 and sgRNA4, listed in Table SI) targeting *PLIN5* exon 4 were designed using an online CRISPR design tool (http://chopchop.cbu.uib.no/). The genotypes of the *PLIN5*$^{-/-}$ mice were amplified by PCR analysis with the knockout (*PLIN5*$^{-/-}$) and wild-type (WT) primer pairs (Table SII). The PCR was performed using the system and program detailed in Tables SIII and SIV by the Nanjing Biomedical Research Institute of Nanjing University (data not shown). Mice were housed in a specific pathogen-free-grade rodent facility, with the temperature maintained at 20-26˚C, relative humidity controlled at 40-70%, and under a 12-h light/dark cycle. Specific pathogen-free-grade C57BL/6J male mice and *PLIN5*$^{-/-}$ male mice (age, 6-7-weeks; weight, ~20 g) were randomly divided into groups fed a normal diet *ad libitum* (ND) or a HFD (n=10/group; n=40 mice total). Mice in the ND group were given a normal chow diet and ultrapure water, whereas those in the HFD group were given a diet high in fat with a 45% fat-supplied ratio (cat. no. H10045; Beijing HFK Bioscience Co., Ltd.) and sugar water for 20 weeks (14). All mice were housed at the Animal Center of Zhengzhou University (Zhengzhou, China) under suitable conditions. For the investigations, the mice were anesthetized via inhalation of isoflurane, employing an initial induction concentration of 4% followed by a maintenance concentration of 1.5%. Once the mice had been fed for 20 weeks, liver specimens were collected and the mice were immediately sacrificed by cervical dislocation under deep anesthesia. Death was confirmed by the cessation of vital signs, including the absence of a palpable heartbeat, fixed and dilated pupils, and unresponsiveness to mechanical stimuli. The Animal Ethics Committee of Zhengzhou University approved the protocols for the animal experiments (approval no. KY2023006). The animals received humane care according to the criteria outlined in the Guide for the Care and Use of Laboratory Animals prepared by the National Academy of Sciences and published by the National Institutes of Health (22).

Cell culture. The murine hepatocyte AML12 cell line was purchased from CHI Scientific, Inc., and was cultured in DMEM/F-12 (1:1) (Gibco; Thermo Fisher Scientific, Inc.) supplemented with 10% fetal bovine serum (cat. no. F8318; MilliporeSigma), 40 ng/ml dexamethasone (to maintain the mature phenotype and specific function of liver cells; cat. no. D4902-25MG; MilliporeSigma) and 100 U/ml penicillin/streptomycin (cat. no. 15140122; Gibco; Thermo Fisher Scientific, Inc.), and incubated at 37˚C with a constant supply

of 5% CO_2. To establish a hepatic steatosis model *in vitro*, AML12 cells were stimulated with palmitic acid (PA; 0.5 mM; cat. no. KC002) and oleic acid (OA; 1.0 mM; cat. no. KC006) (both from Kun Chuang Biotechnology) [dissolved in 0.5% fatty acid-free bovine serum albumin (BSA); cat. no. KC002; Kun Chuang Biotechnology] at the indicated concentrations for 48 h. The control group was treated with 0.5% fatty acid-free BSA (21).

Biochemical analysis. To assess the antioxidant capacity of the mouse liver samples from five mice per group and AML12 cells, commercial assay kits (Wuhan Elabscience Biotechnology Co., Ltd.) were used to measure the levels of glutathione (GSH; cat. no. E-BC-K030-M) and malondialdehyde (MDA; cat. no. E-BC-K025-M), according to the manufacturer's instructions. To measure the levels of ferroptosis in mice, the Cell Ferrous Iron (Fe^{2+}) Fluorometric Assay Kit (cat. no. E-BC-F101; Wuhan Elabscience Biotechnology Co., Ltd.) was used to detect levels of Fe^{2+}, according to the manufacturer's instructions.

RNA sequencing (RNA-seq) and bioinformatics analysis. When the AML12 cell density reached ~70% confluence, the cells were stimulate with PA (0.5 mM) and OA (1.0 mM) at 37˚C for 48 h, and continuously supply 5% CO_2. Following treatment, the cells were lysed with TRIzol® reagent (cat. no. 15596026; Invitrogen; Thermo Fisher Scientific, Inc.) and homogenized via repetitive pipetting. Total RNA was isolated using chloroform phase separation followed by isopropanol precipitation. RNA integrity was verified using an Agilent Bioanalyzer 2100 system (RNA integrity number >8.0; Agilent Technologies, Inc.), and purity was confirmed using a NanoDrop spectrophotometer (A260/A280 ratio ≥1.9; NanoDrop; Thermo Fisher Scientific, Inc.). RNA-seq library preparation and paired-end sequencing (150 bp) were performed by Shanghai OE Biotech Co., Ltd., using an Illumina NovaSeq 6000 platform (Illumina, Inc.) with the NovaSeq 6000 S4 Reagent Kit (300 cycles; cat. no. 20027466; Illumina, Inc.), The loading concentration of the final library was adjusted to 10-20 pM, according to standardized protocols. The raw RNA-seq data generated in the current study have been deposited in the NCBI Sequence Read Archive under accession number PRJNA1295086 (https://www.ncbi.nlm.nih.gov/bioproject/PRJNA1295086/).

Using the GeneCards database (https://www.genecards.org/), an association between PLIN5 and ferroptosis was searched for using the key words 'PLIN5' and 'ferroptosis'. Gene set enrichment analysis was performed using the Gene Ontology (GO; http://geneontology.org/) and Kyoto Encyclopedia of Genes and Genomes (KEGG; https://www.kegg.jp//) databases. Protein-protein interaction (PPI) network analysis was carried out using the STRING database (https://string-db.org/).

Single-cell RNA-seq. Once the mice had been fed for 20 weeks, liver tissues from five randomly selected mice in each group were used for single-cell RNA-seq. Livers were perfused with collagenase IV/DNase I and incubated at 37˚C for 15-30 min. Cells were then filtered through a 40-μm strainer and viable cells were enriched via flow cytometry (CytoFLEX S V4-B2-Y4-RO; Beckman Coulter, Inc.). Single-cell capture, cDNA library construction and sequencing were performed by Shanghai Bohao Biotechnology Co., Ltd., using the 10x Genomics Chromium platform (targeting 5,000-10,000 cells/sample; 10x Genomics, Inc.) with the 10x Genomics Chromium Next GEM Single Cell 3'Reagent Kit v3.1 (cat. no. 1000268; 10x Genomics, Inc.), according to standardized protocols. An Agilent Bioanalyzer 2100 System (Agilent Technologies, Inc.) was used to detect sample integrity. The final loading concentration of the library was ≥10 pM, and the sequencing was performed using a paired-end strategy with a read length of 150 bp. Raw sequencing data were deposited in the China National Center for Bioinformation under accession number CRA018673 (https://ngdc.cncb.ac.cn/gsa/search?searchTerm=CRA018673).

The DESeq2 package (1.34.0; https://bioconductor.org/packages/release/bioc/html/DESeq2.html) was used to identify differentially expressed genes (DEGs); genes with a P-value <0.05 and $|\log_2$ fold-change (FC)$|>1$ were defined as DEGs. A volcano map of the DEGs was generated using the ggplot2 (https://ggplot2.tidyverse.org/) in R. DEGs and ferroptosis-related genes from the FerrDb database (http://www.zhounan.org/ferrdb) were collated into Venn diagrams; overlapping DEGs were selected for subsequent analyses.

Reverse transcription-quantitative polymerase chain reaction (RT-qPCR). RNA extraction from AML12 cells and mouse liver tissue from five mice per group was performed using a Cell/Tissue Total RNA Rapid Extraction Kit (Novogene Co., Ltd.), according to the manufacturer's instructions. The extracted RNA was then reverse-transcribed into cDNA using an RT kit (Toyobo Co., Ltd.) according to the manufacturer's protocol. Subsequently, cDNA, primers and SYBR Green Master Mix (Toyobo Co., Ltd.) were combined in the appropriate proportions, and PCR amplification was carried out using the LightCycler 480 system (Roche Diagnostics). qPCR was performed using a three-step protocol, as follows: Initial denaturation at 95˚C for 10 min for 1 cycle; 35 cycles of denaturation at 95˚C for 15 sec, annealing at 60˚C for 15 sec and extension at 72˚C for 45 sec; and a final extension step at 72˚C for 7 min for 1 cycle. The relative abundance of mRNA was normalized to *GAPDH* mRNA. Gene expression levels were calculated using the $2^{-\Delta\Delta Cq}$ method. The data are expressed as the ratio of the mean of three independent repeats, and each experiment was repeated at least three times. The primers used for qPCR are listed in Table SV.

Western blotting (WB). Total protein was extracted from AML12 cells and mouse liver tissues from three mice per group using high-efficiency radioimmunoprecipitation assay lysis buffer containing protease inhibitors (Beijing Solarbio Science & Technology Co., Ltd.). Protein concentrations were measured using a BCA Protein Assay Kit (Beijing Solarbio Science & Technology Co., Ltd.). Subsequently, proteins (20 μg/lane) were separated by SDS-PAGE on 10% gels and were transferred to nitrocellulose membranes (Pall Life Sciences), which were blocked with 8% skim milk in Tris-buffered saline containing 0.1% Tween-20 (TBST) for 2 h at room temperature. The membranes were then incubated overnight at 4˚C with primary antibodies, and after washing with TBST, the membranes were incubated with HRP-conjugated AffiniPure Goat Anti-rabbit

IgG (H + L) secondary antibodies at room temperature for 2 h, before being washed in TBST. The target proteins were detected using enhanced chemiluminescence (ECL) detection reagent (Epizyme; Ipsen Pharma) and signal intensities were captured using an ECL western-blotting analysis system (Tanon Science and Technology Co., Ltd.). Semi-quantitative analysis was performed using ImageJ version 1.8.0t software (National Institutes of Health). All primary and secondary antibodies used are listed in Table SVI.

Plasmid transfection. *PLIN5* overexpression and *ATF3* knockdown plasmids, along with their corresponding negative controls, were commercially obtained from Suzhou GenePharma Co., Ltd. The *PLIN5* overexpression plasmid was constructed using the pcDNA3.1(+) backbone, while the *ATF3* short hairpin (sh)RNA and its scrambled negative control were cloned into the pGPU6/GFP/Neo plasmid. For transient transfection, AML12 cells were seeded at a density of $2.5x10^5$ cells/well in 6-well plates and cultured for 24 h to reach 70-80% confluence. Transfection was performed using Lipofectamine® 3000 reagent (Invitrogen; Thermo Fisher Scientific, Inc.) according to the manufacturer's instructions. Specifically, 2.5 μg plasmid DNA and 5 μl Lipofectamine 3000 reagent were diluted separately in Opti-MEM (cat. no. 31985070; Gibco; Thermo Fisher Scientific, Inc.), then combined and incubated for 15 min at room temperature to form transfection complexes. The complexes were added dropwise to the cells, which were then incubated at 37˚C in a 5% CO_2 environment. The culture medium was replaced with fresh medium at 6 h, and after 48 h of total incubation, the cells were harvested for subsequent experiments. The sequences of shRNAs are listed in Table SVII. The negative control used for overexpression consisted of an empty pcDNA3.1(+) vector, whereas a non-targeting scrambled shRNA was used as the control for knockdown experiments. Following transfection, the cells were treated with PAOA for 48 h. In addition, in the pcDNA3.1 *PLIN5* + ferrostatin-1 (FER-1) group, the cells were transfected with pcDNA3.1 *PLIN5,* pretreated with 2 μM FER-1 (cat. no. HY-100579; MedChemExpress) at 37˚C in a 5% CO_2 cell culture incubator for 1 h, and then treated with PAOA for an additional 48 h.

Oil red O (ORO) staining. AML12 cells were cultured in a 6-well plate and then fixed with 4% paraformaldehyde at room temperature for 30 min, followed by staining with ORO staining solution for 30 min at room temperature (Nanjing Jiancheng Bioengineering Institute), according to the manufacturer's instructions. Subsequently, the cells were thoroughly rinsed with distilled water to remove unbound dye and images were acquired using a light microscope (Nikon Corporation). Quantification of the staining results was conducted using ImageJ (version 1.8.0).

FerroOrange staining. AML12 cells were fixed with 4% paraformaldehyde at room temperature for 15 min. After washing, the nuclei were stained with the nuclear dye green cyanine SYTO (Jiangsu Kaiji Biotechnology) for 10 min at room temperature. Subsequently, Fe^{2+} was detected by incubating the cells with FerroOrange dye (Tocris Bioscience) for 30 min at 37˚C in the dark. Cellular nuclei and Fe^{2+} signals were visualized using a confocal microscope (Zeiss LSM 900; Carl Zeiss AG). All experimental procedures were carried out according to the instructions provided with the reagents.

H&E staining. Histological analysis was performed on liver tissues from three mice per group fixed in 4% paraformaldehyde for 24 h at room temperature, followed by paraffin embedding and slicing into 5-μm sections. The sections were then deparaffinized in xylene and rehydrated through a graded ethanol series (100, 95, 85 and 70%) to distilled water. Subsequently, nuclei were stained with Harris hematoxylin for 5 min at room temperature, differentiated in 1% acid alcohol and blued in Scott's tap water. The cytoplasm and extracellular matrix were counterstained with eosin Y for 2 min at room temperature. Finally, sections were dehydrated through a graded ethanol series, cleared in xylene and mounted with neutral balsam. Histopathological examination was conducted using a light microscope (Nikon Corporation).

Masson's trichrome staining. Histological analysis was performed on liver tissues from three mice per group fixed in 4% paraformaldehyde for 24 h at room temperature, followed by paraffin embedding and slicing into 5-μm sections. All staining procedures were carried out at room temperature. Sections were stained with Weigert's hematoxylin (5-10 min), 1% eosin ethanol (5 min) and Masson composite solution (5 min), followed by differentiation in 1% hydrochloric acid ethanol (30 sec) and 2% acetic acid (30 sec). Dehydration was performed using graded ethanol series (70, 85, 95 and 100%). Finally, histopathological images were acquired using a light microscope (Nikon Corporation).

TG analysis. The concentration of TGs of mouse liver tissues from five mice per group was quantified using a commercial TG assay kit (cat. no. BC0625; Beijing Solarbio Science & Technology Co., Ltd.) in accordance with the manufacturer's protocol. TG was extracted with isopropanol and subsequently saponified using KOH to release glycerol and free fatty acids. The liberated glycerol was oxidized by iodine to generate formaldehyde, which then underwent condensation with acetylacetone in the presence of chloride ions to yield a yellow-colored product. This chromophore displays a distinct absorption peak at 420 nm, and the absorbance intensity is proportional to the original TG concentration. This well-established method allows accurate and reproducible determination of TG levels.

Total cholesterol (TC) analysis. The concentration of TC in mouse liver tissues from five mice per group was determined using a commercial TC assay kit (cat. no. BC1985; Beijing Solarbio Science & Technology Co., Ltd.) according to the manufacturer's instructions. The extracted cholesterol esters were first hydrolyzed to free cholesterol by cholesterol esterase. The free cholesterol was then oxidized by cholesterol oxidase to generate hydrogen peroxide. In the presence of peroxidase, hydrogen peroxide reacted with 4-aminoantipyrine and phenol to form a red quinoneimine dye. The absorbance of this colored product was measured at 500 nm, and its intensity is proportional to TC concentration.

Alanine aminotransferase (ALT) analysis. The concentration of ALT was determined using a commercial ALT assay kit (cat. no. BC1555; Beijing Solarbio Science & Technology Co., Ltd.) according to the manufacturer's instructions. After mouse anesthesia, as aforementioned, whole blood (~500 μl/mouse) was collected from the retro-orbital plexus of the 40 mice using sterile glass capillary tubes (cat. no. 71900-10; KIMBLE®; DWK Life Sciences) and immediately transferred to 1.5-ml microcentrifuge tubes. The mice were subsequently sacrificed by cervical dislocation under deep anesthesia. The blood was allowed to clot at room temperature for 30 min and the clots were then pelleted by centrifugation at 2,000 x g for 15 min at 4˚C. Subsequently, the supernatant (serum) was carefully aspirated, aliquoted and stored at -80˚C until further analysis.

The serum samples from five mice per group were diluted with physiological saline at a ratio of 1:10. A total of 5 μl serum was mixed with 290 μl working reagent containing Tris buffer (pH 7.8), L-alanine, α-ketoglutarate, NADH and lactate dehydrogenase. The samples were incubated at 37˚C for 30 min to allow the enzyme to fully react with the substrate. After the reaction was complete, 50 μl NADH chromogenic reagent was added to each well, and the OD value change was measured at a wavelength of 505 nm. ALT activity in the sample was calculated based on the standard curve.

Statistical analysis. Data are presented as the mean ± standard error of mean of at least three independent experiments. All statistical analyses were performed using GraphPad Prism software version 9.5.1 (Dotmatics), and data were analyzed using one-way analysis of variance followed by Bonferroni's post hoc test. $P<0.05$ was considered to indicate a statistically significant difference.

Results

PLIN5 deficiency inhibits ferroptosis in lipotoxic hepatocytes in vitro and in vivo. First, an *in vitro* PAOA-induced hepatocyte steatosis model was constructed by treating AML12 cells with PAOA for 48 h. RNA was collected for transcriptome sequencing, and gene set enrichment analysis with GO and KEGG was performed to analyze the cell signaling pathways involved in lipid accumulation and inflammation. The results revealed that PAOA treatment activated signaling pathways associated with lipid accumulation and inflammation, such as 'fatty acid metabolic process', 'response to lipopolysaccharide', 'response to fatty acid', 'immune response', 'inflammatory response', 'innate immune response', 'IL-17 signaling pathway, 'NF-kappa B signaling pathway' and 'TNF signaling pathway' (Fig. S1B and D). In addition, using ORO staining to assess LD content, followed by statistical analysis with ImageJ, the LD content was markedly increased in PAOA-treated AML12 cells compared with that in the BSA control group (Fig. S1A). These data indicated that the lipotoxic cell model was successfully constructed. Furthermore, the expression levels of PLIN5 were increased in AML12 cells treated with PAOA compared with those in the BSA group (Fig. S1E and F).

To investigate the impact of PLIN5 on ferroptosis under lipotoxic conditions, the key words 'PLIN5' and 'ferroptosis' were searched in the GeneCards database to determine their association. A total of 113 genes were identified to be associated with both PLIN5 and ferroptosis. According to GO enrichment analysis, the significantly regulated terms were primarily related to ferroptosis and lipid metabolism signaling, such as 'ferroptosis', 'PPAR signaling pathway' and 'fatty acid biosynthesis', indicating that these genes were not only associated with ferroptosis, but were also closely related to biological processes such as lipid metabolism (Fig. S1C). The primary changes in biochemical characteristics associated with ferroptosis are iron overload and decreased activity of the ferroptosis marker gene GSH peroxidase 4 (*GPX4*) in MAFLD development (23,24). In the present study, PPI analysis revealed an indirect association between PLIN5 and GPX4 (Fig. S1G).

The present study revealed that PAOA-treated AML12 cells exhibited elevated Fe^{2+} and significantly reduced GPX4 expression under lipotoxic conditions compared with those in the BSA group (Fig. 1A and B), indicating that PAOA treatment induced ferroptosis *in vitro*. Notably, Fe^{2+} levels were significantly decreased in the livers of mice in the *PLIN5*$^{-/-}$ HFD group compared with those in the WT HFD group (Fig. 1C). The successful knockout of *PLIN5* is shown in Fig. S2A and B. It has previously been reported that patients with MAFLD have elevated levels of the lipid peroxidation marker MDA (25). The current study also measured the redox markers MDA and GSH in the liver tissues from WT and *PLIN5*$^{-/-}$ mice fed a ND or HFD for 20 weeks. After HFD feeding, MDA was increased and GSH was significantly decreased in mice from both groups; by contrast, MDA levels were significantly decreased and GSH levels were significantly increased in the *PLIN5*$^{-/-}$ HFD group compared with those in the WT HFD group (Fig. 1D and E).

Notably, GPX4 expression levels were significantly higher in the liver tissues of the *PLIN5*$^{-/-}$ HFD group compared with those in the WT HFD group (Fig. 1F and G). Consistent with our previous reports (10,11). H&E staining revealed a marked reduction in lipid droplets in the *PLIN5*$^{-/-}$ group compared with those in the WT group (Fig. S2C). Furthermore, Masson's trichrome staining indicated a decrease in liver fibrosis in *PLIN5*$^{-/-}$ mice (Fig. S2D), and TG and TC levels were significantly reduced compared with those in the WT group (Fig. S2E and F). Additionally, serum ALT levels were lower in the *PLIN5*$^{-/-}$ group compared with those in the WT group (Fig. S2G). These findings indicated that *PLIN5* knockout could attenuate hepatic steatosis and injury, and suggested that *PLIN5* deficiency may delay the progression of MAFLD in mice by inhibiting ferroptosis.

Overexpression of PLIN5 promotes lipid accumulation and ferroptosis in hepatocytes. To further explore how PLIN5 affects ferroptosis, a *PLIN5* overexpression cell model was established (Fig. 2A and B). *PLIN5*-overexpressing cells were pretreated with FER-1, a selectively effective inhibitor of ferroptosis, and all cell groups were treated with PAOA. The results showed that LD accumulation was significantly increased in the pcDNA3.1-*PLIN5* group compared with that in the pcDNA3.1 group, which was reversed by the addition of FER-1 (Fig. 2C). Furthermore, Fe^{2+} fluorescence intensity was significantly enhanced in the pcDNA3. 1-*PLIN5* group treated with PAOA, which was reversed by the addition of FER-1 (Fig. 2D). Furthermore, the MDA content was increased and GSH levels were significantly decreased in pcDNA3.1-*PLIN5*

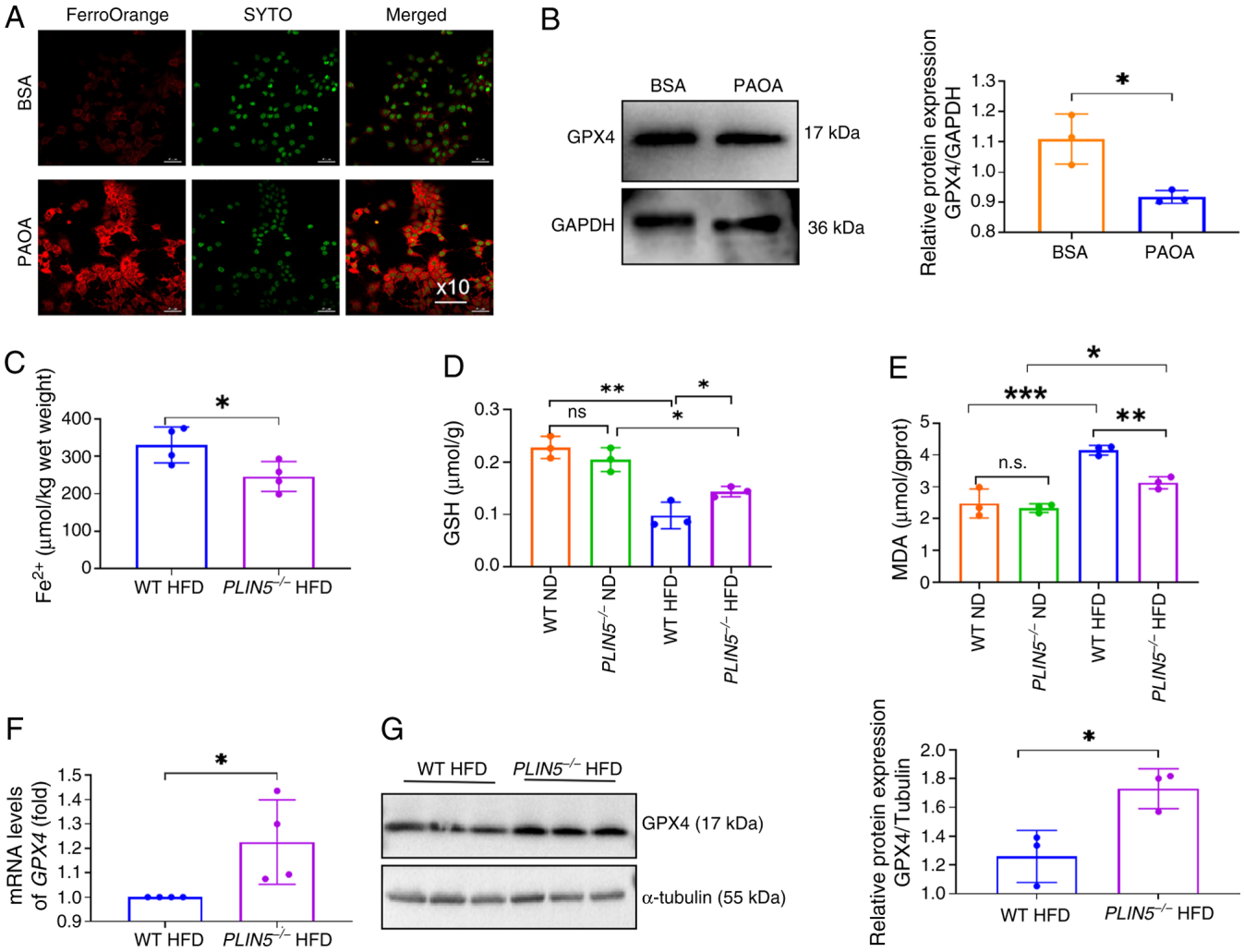

Figure 1. *PLIN5* deficiency inhibits ferroptosis in lipotoxic hepatocytes *in vitro* and *in vivo*. (A) Fe^{2+} fluorescence intensity in AML12 cells observed using a fluorescence microscope (magnification, x10), with red indicating Fe^{2+} fluorescence and green indicating nuclei. (B) Western blot analysis of GPX4 protein expression in BSA- or PAOA-treated cells was performed, with GAPDH used as an internal control. (C) Fe^{2+} content in the livers of mice in the WT HFD group and *PLIN5*$^{-/-}$ HFD group was measured (n=5 mice/group). (D) Liver GSH content of mice in each group was detected (n=5 mice/group). (E) Liver MDA content of mice in each group was detected (n=5 mice/group). (F) mRNA levels of *GPX4* in the liver tissues of mice in the WT HFD and *PLIN5*$^{-/-}$ HFD groups were analyzed by quantitative polymerase chain reaction (n=5 mice/group). (G) Western blot analysis of GPX4 protein expression in the liver tissues of mice from the WT HFD and *PLIN5*$^{-/-}$ HFD groups was performed, with tubulin used as an internal control (n=3 mice/group). All experiments were repeated at least three times (n=3). *P<0.05, **P<0.01, ***P<0.001, n.s., not significant. Fe^{2+}, ferrous ion; GSH, glutathione; GPX4, GSH peroxidase 4; HFD, high-fat diet; MDA, malondialdehyde; PAOA, palmitic acid and oleic acid; PLIN5, perilipin 5; WT, wild-type.

cells treated with PAOA, which was reversed by treatment with FER-1 (Fig. 2E and F). These findings revealed that *PLIN5* overexpression could promote lipid accumulation and ferroptosis in PAOA-treated hepatocytes, and that the ferroptosis inhibitor FER-1 could partially alleviate lipid accumulation, oxidative damage and FE^{2+} content caused by *PLIN5* overexpression.

PLIN5-induced ferroptosis is associated with ATF3. As aforementioned, the present study initially discovered that PLIN5 may modulate ferroptosis both *in vivo* and *in vitro*. To further elucidate how PLIN5 affects ferroptosis signaling, an in-depth analysis was subsequently performed by mining single-cell RNA-seq data. This strategy enabled identification of cell type-specific ferroptosis regulators downstream of PLIN5. The current study analyzed single-cell RNA-seq data obtained from the liver tissues from 5 mice from the *PLIN5*$^{-/-}$ HFD group and 5 mice from the WT HFD group to elucidate the functional genes involved in regulating the effects of *PLIN5* knockout in MAFLD. The results revealed that there were 235 DEGs (log_2 FC>1, P<0.05) between the *PLIN5*$^{-/-}$ HFD and WT HFD groups, with 110 upregulated and 125 downregulated genes (Fig. 3A). Notably, these genes were intersected with the FerrDb database and seven ferroptosis-related DEGs were identified, including two upregulated genes: Fascin actin-bundling protein 1 (*FSCN1*) and *MYC*, and five downregulated genes: *ATF3*, glycerophosphodiester phosphodiesterase domain containing 5 (*GDPD5*), lactotransferrin (*LTF*), *PLIN2* and protein regulator of cytokinesis 1 (*PRC1*) (Fig. 3B). GO and KEGG analyses were performed on the aforementioned genes (Fig. 3C). The DEGs associated with ferroptosis were involved in various biological processes, including 'carboxylic acid transport', 'organic acid transport' and 'monocarboxylic acid transport'. The genes were enriched in molecular

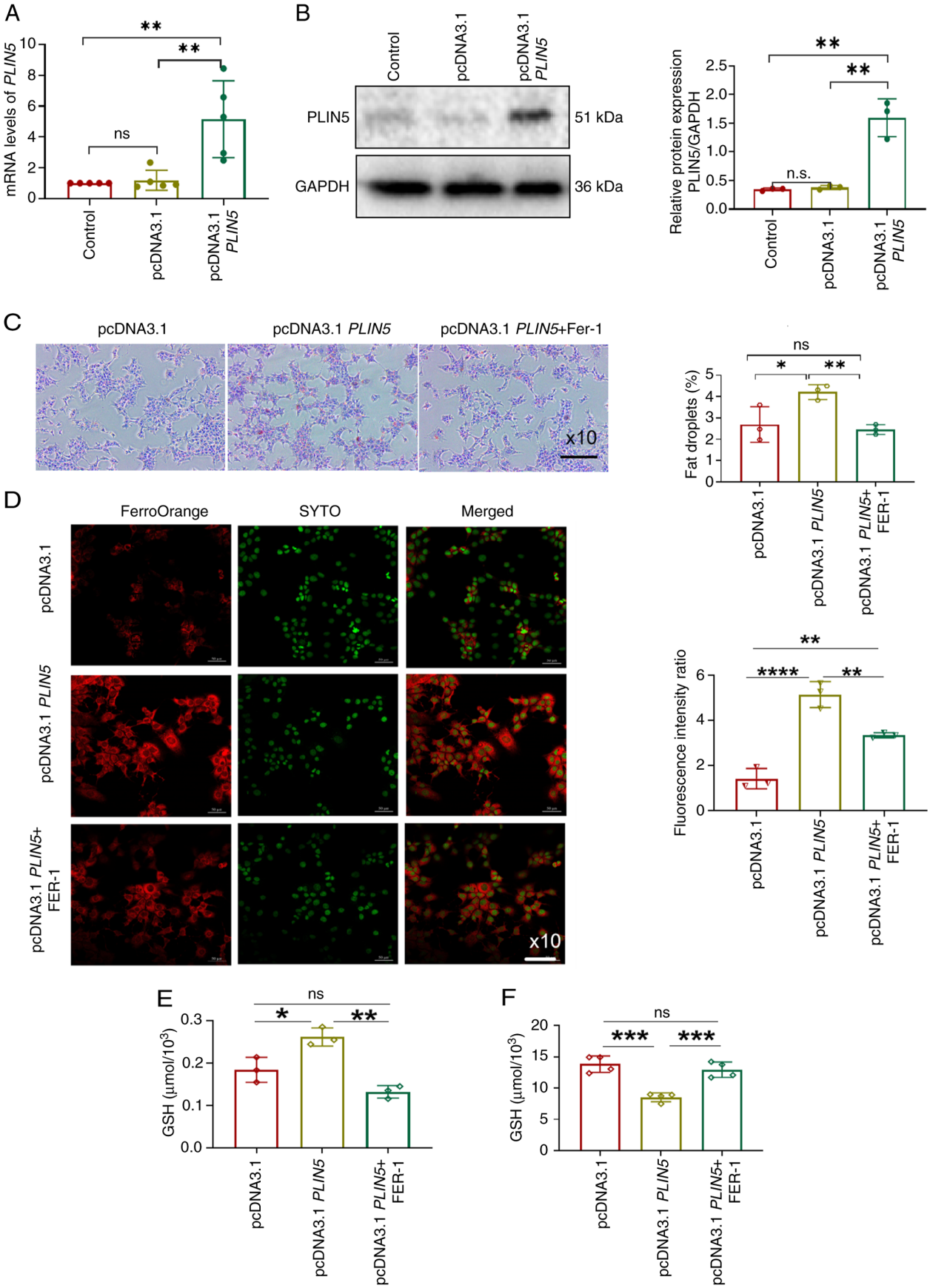

Figure 2. Overexpression of *PLIN5* promotes lipid accumulation and ferroptosis in hepatocytes. (A) mRNA levels of *PLIN5* levels were detected via quantitative polymerase chain reaction. (B) PLIN5 protein expression was detected via western blotting. (C) LD changes in cells were observed using a microscope (magnification, x10), with nuclei stained blue and LDs stained red. Quantitative analysis was performed using ImageJ. (D) Fe^{2+} fluorescence intensity in cells was observed using a fluorescence microscope (magnification, x10), with nuclei stained green and Fe^{2+} fluorescence stained red, followed by quantitative analysis. (E) MDA levels were detected in the three cell groups. (F) GSH levels were detected in the three groups of cells. *P<0.05, **P<0.01, ***P<0.001, ****P<0.0001, n.s., not significant. Fe^{2+}, ferrous ion; GSH, glutathione; LD, lipid droplet; MDA, malondialdehyde; PLIN5, perilipin 5; FER-1, ferrostatin-1.

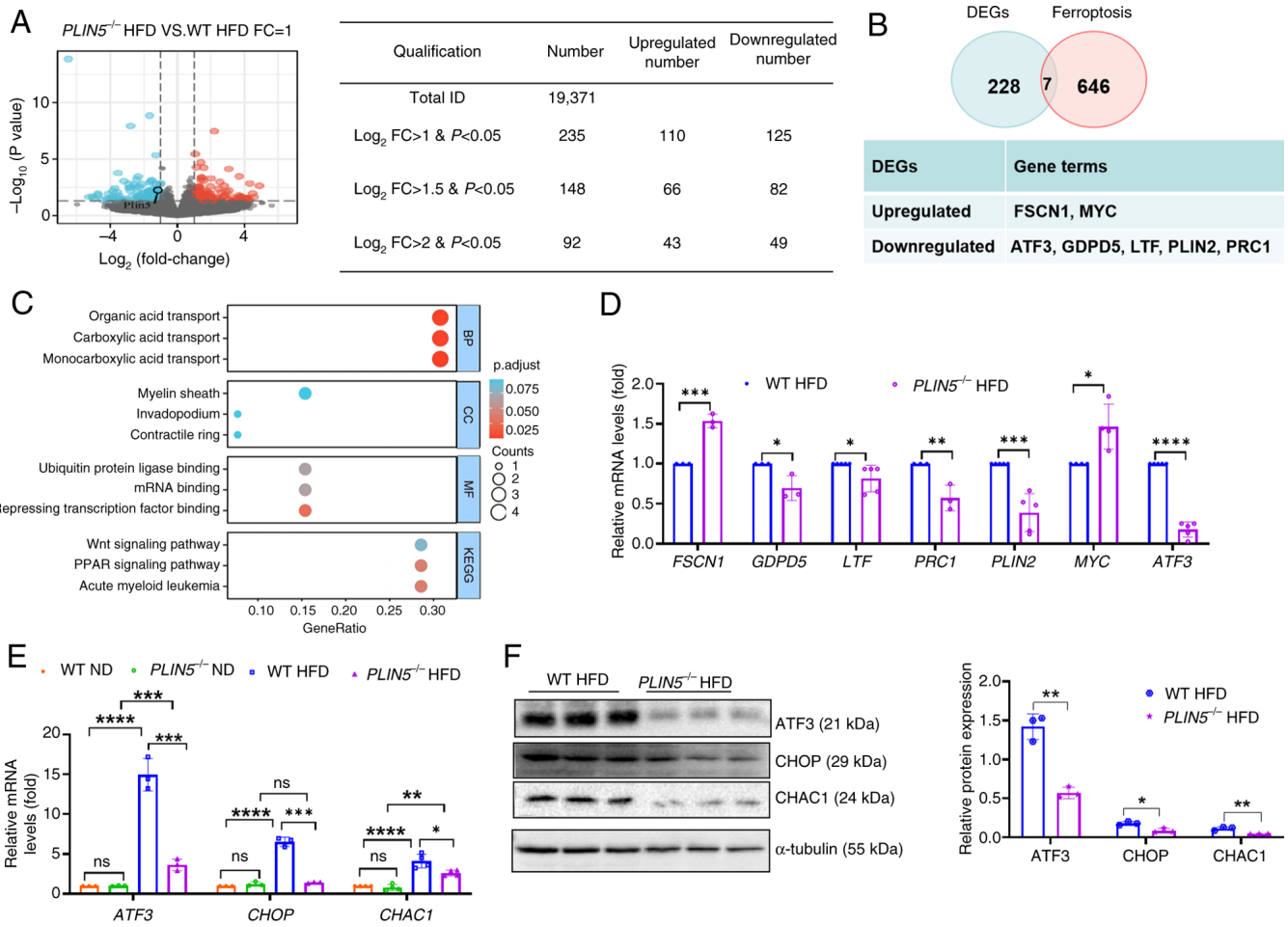

Qualification	Number	Upregulated number	Downregulated number
Total ID	19,371		
Log_2 FC>1 & *P*<0.05	235	110	125
Log_2 FC>1.5 & *P*<0.05	148	66	82
Log_2 FC>2 & *P*<0.05	92	43	49

DEGs	Gene terms
Upregulated	FSCN1, MYC
Downregulated	ATF3, GDPD5, LTF, PLIN2, PRC1

Figure 3. *PLIN5* affects ferroptosis through ATF3/CHOP/CHAC1 signaling. (A) DEGs in mouse liver tissues from the *PLIN5*$^{-/-}$ HFD group are shown compared to those in the WT HFD group (red dots represent upregulated genes, whereas blue dots represent downregulated genes). (B) DEGs associated with ferroptosis in the *PLIN5*$^{-/-}$ HFD and WT HFD groups were analyzed (log_2 FC>1, P<0.05). (C) KEGG pathway and GO term enrichment analyses of different genes were performed. (D) mRNA levels of *PRC1, LTF, GDPD5, FSCN1, MYC, ATF3* and *PLIN2* in the liver tissues of WT HFD and *PLIN5*$^{-/-}$ HFD mice were measured (n=5 mice/group). (E) mRNA levels of *ATF3*, *CHOP* and *CHAC1* in the liver tissues of mice in each group were detected (n=5 mice/group). (F) Western blot analysis of ATF3, CHOP and CHAC1 protein expression in the liver tissues of mice from the WT HFD and *PLIN5*$^{-/-}$ HFD groups was performed, with tubulin as the internal reference. Semi-quantitative analysis performed using ImageJ (n=3 mice/group). All experiments were repeated at least three times (n=3). *P<0.05, **P<0.01, ***P<0.001, ****P<0.0001, n.s., not significant. ATF3, activating transcription factor 3; CHAC1, cation transport regulator-like protein 1; CHOP, C/EBP homologous protein; DEGs, differentially expressed genes; FC, fold-change; *FSCN1*, fascin actin-bundling protein 1; *GDPD5*, glycerophosphodiester phosphodiesterase domain containing 5; *GPX4*, glutathione peroxidase 4; HFD, high-fat diet; KEGG, Kyoto Encyclopedia of Genes and Genomes; ND, normal diet; *LTF*, lactotransferrin; *PLIN*, perilipin; *PRC1*, protein regulator of cytokinesis 1; WT, wild-type; BP, biological process; CC, cellular component; MF, molecular function.

functions related to 'repressing transcription factor binding', 'mRNA binding' and 'ubiquitin protein ligase binding'. In addition, these DEGs were enriched in the following cellular components: 'Myelin sheath', 'contractile ring' and 'invadopodium'. KEGG analysis revealed associations with 'acute myeloid leukemia', as well as the 'PPAR signaling pathway' and 'Wnt signaling pathway'. The results of RT-qPCR showed that, compared with those in the WT HFD group, the mRNA expression levels of *FSCN1* (P<0.001) and *MYC* (P<0.05) were significantly higher in the *PLIN5*$^{-/-}$ HFD group, whereas the mRNA levels of *ATF3*, *GDPD5* (P<0.05), *LTF*, *PLIN2* and *PRC1* were significantly lower; among these, the most significant difference was observed in *ATF3*) (Fig. 3D). Therefore, *PLIN5* knockout-induced inhibition of ferroptosis in MAFLD may be associated with *ATF3*.

ATF3 is a member of the ATF/CREB transcription factor family and is upregulated in mouse models of non-alcoholic steatohepatitis (NASH) (26). The C/EBP homologous protein (CHOP) signaling pathway is involved in the synergistic interaction between ferroptosis and apoptosis (27). ATF3 and CHOP regulate the transcription of cation transport regulator-like protein 1 (CHAC1) (28), and elevated CHAC1 is an important marker of ferroptosis (29,30). Notably, the present results showed that the expression levels of ATF3, CHOP and CHAC1 were significantly lower in the *PLIN5*$^{-/-}$ HFD group compared with those in the WT HFD group, and compared with in the ND group, their expression levels were significantly increased in the HFD group (Fig. 3E and F). Moreover, single-cell transcriptome data were analyzed and it was revealed that knocking out *PLIN5* significantly reduced the expression of *ACSL4* in hepatocytes in *PLIN5*$^{-/-}$ HFD mice compared with that in the WT HFD group; however, there was no difference in the expression of *SLC7A11* (Fig. S3). These findings suggested that knocking out *PLIN5* can inhibit ferroptosis. Notably,

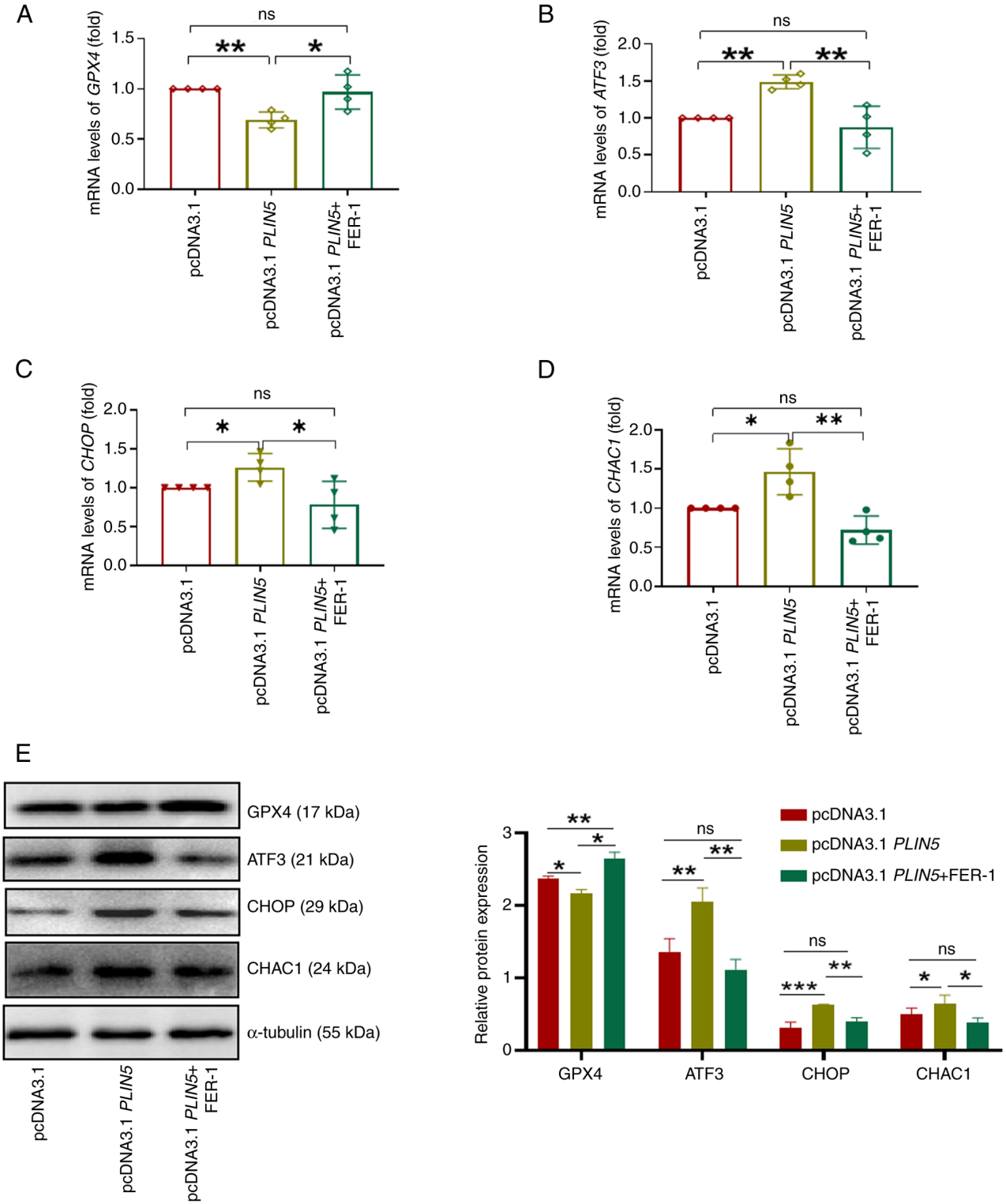

Figure 4. *PLIN5* affects ferroptosis via ATF3/CHOP/CHAC1 signaling. The mRNA expression levels of (A) *GPX4*, (B) *ATF3*, (C) *CHOP* and (D) *CHAC1* in cells from each group were measured. (E) Western blot analysis of GPX4, ATF3, CHOP and CHAC1 protein expression in cells from different groups was performed, normalized to tubulin as an internal control. Semi-quantitative analysis was performed using ImageJ. All experiments were repeated at least three times. *P<0.05, **P<0.01, ***P<0.001, n.s., not significant. ATF3, activating transcription factor 3; CHAC1, cation transport regulator-like protein 1; CHOP, C/EBP homologous protein; FER-1, ferrostatin-1; *GPX4*, glutathione peroxidase 4; PAOA, palmitic acid and oleic acid; *PLIN5*, perilipin 5.

overexpression of *PLIN5* could promote the expression of, *ATF3*, *CHOP* and *CHAC1* with PAOA treatment compared with that in the pcDNA3.1 group, which was reversed by FER-1 treatment (Fig. 4B-E). By contrast, compared with those in the pcDNA3.1 group, GPX4 expression levels were significantly decreased by *PLIN5* overexpression; however, GPX4 was significantly enhanced in the pcDNA3.1 *PLIN5* + FER-1 group (Fig. 4A and E). Taken together, these findings suggested that ATF3 may be involved in the PLIN5-associated regulation of HFD-induced hepatocyte ferroptosis.

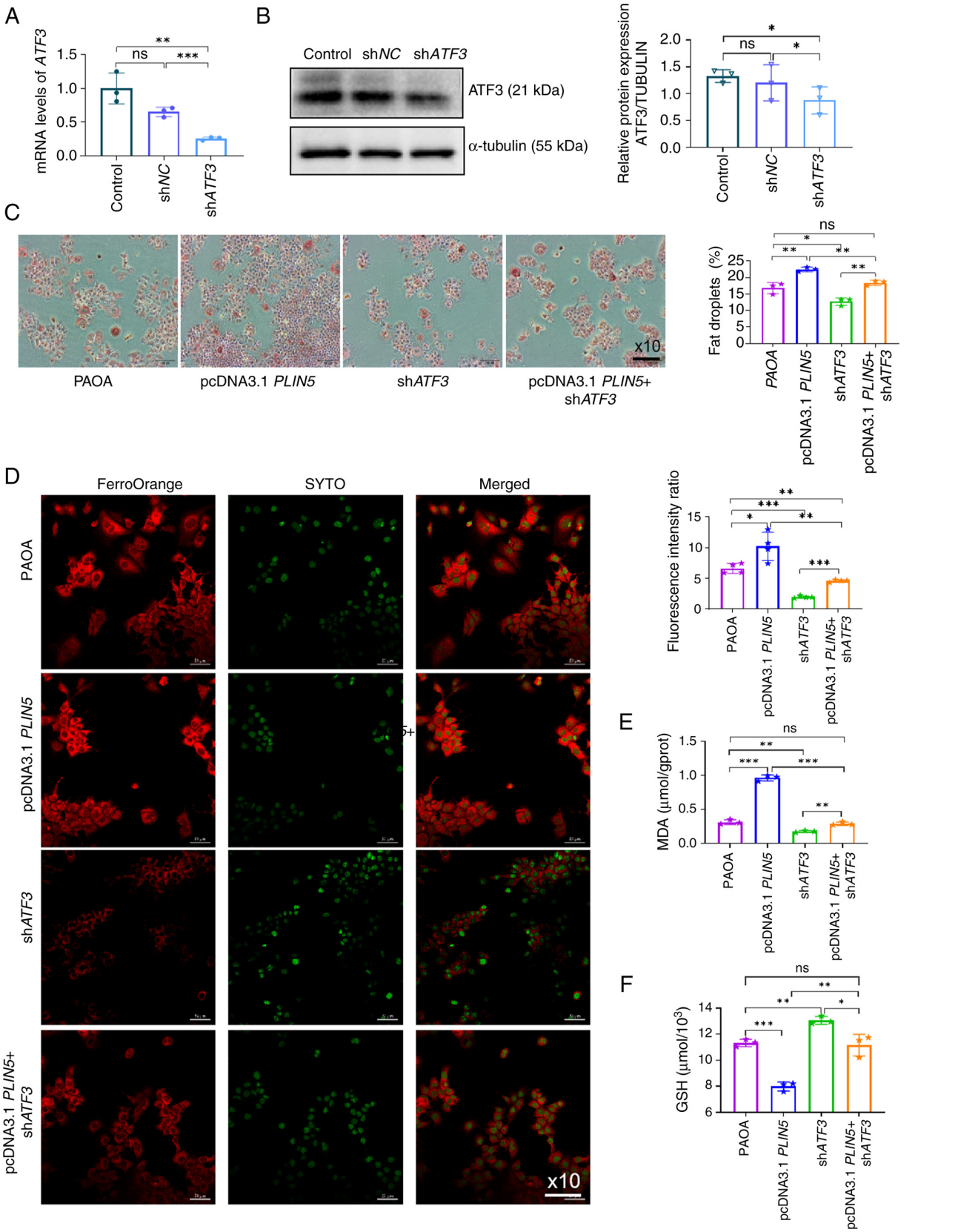

Figure 5. Knockdown of *ATF3* alleviates lipid accumulation and ferroptosis induced by overexpression of *PLIN5*. (A) *ATF3* mRNA expression in AML12 cells was analyzed by quantitative polymerase chain reaction 48 h after transfection with shATF3 plasmid. (B) Semi-quantitative analysis of ATF3 protein expression in AML12 cells 48 h after transfection with shATF3 plasmid was performed, normalized to tubulin as an internal control, using ImageJ. (C) LDs were observed in cells from different intervention groups using a microscope (magnification, x10), with nuclei stained blue and LDs stained red and quantitative analysis was performed using ImageJ. (D) Fe^{2+} fluorescence intensity in cells from different intervention groups was observed using a fluorescence microscope, with nuclei stained green and Fe^{2+} fluorescence stained red, followed by quantitative analysis. (E) MDA content was measured in cells from different intervention groups. (F) GSH content was measured in cells from different intervention groups. All experiments were repeated at least three times. *P<0.05, **P<0.01, ***P<0.001, n.s., not significant. ATF3, activating transcription factor 3; Fe^{2+}, ferrous ion; GSH, glutathione; LD, lipid droplet; MDA, malondialdehyde; NC, negative control; PAOA, palmitic acid and oleic acid; *PLIN5*, perilipin 5; sh, short hairpin.

Knockdown of ATF3 alleviates lipid accumulation and ferroptosis induced by overexpression of PLIN5. To confirm that ATF3 is involved in the process of PLIN5-regulated ferroptosis, ATF3 expression was knocked down in the cells (Fig. 5A and B). PAOA stimulation was used to establish cell models, and then ORO staining was performed. The results showed that *ATF3* knockdown significantly reduced PAOA-induced lipid accumulation in hepatocytes and also partially reversed lipid accumulation induced by *PLIN5* overexpression (Fig. 5C). In addition, *ATF3* knockdown partially reversed the Fe^{2+} fluorescence intensity induced by PLIN5 overexpression, and PAOA-induced oxidative damage was also alleviated, as determined by MDA and GSH detection (Fig. 5D-F). Collectively, these results suggested that as a key regulator, PLIN5 could enhance lipid peroxidation and ferroptosis in hepatocytes.

Discussion

Over time, the increasing incidence of MAFLD and associated complications leading to mortality have become of increasing concern (31). The development of MAFLD is associated with lipid accumulation, oxidative stress, ERS and lipotoxicity (4). The pathogenesis of MAFLD is complex, and there are currently no specific drugs that can be used to reverse MAFLD. Notably, different types of hepatocellular death in MAFLD, including apoptosis, necrosis, necroptosis and pyroptosis, have been studied extensively (32,33). Ferroptosis is a form of regulated cell death that is iron-dependent and non-apoptotic, induced by lipid peroxidation and controlled by the integration of oxidative and antioxidant systems (34). Key steps in the formation of ferroptosis include Fe^{2+} accumulation and lipid peroxidation, and ACSL4 and GPX4 positively and negatively regulate ferroptosis, respectively (24,25).

Previous studies have shown that ferroptosis is exacerbated in MAFLD, that it serves an important role as a trigger for the initiation of inflammation in steatohepatitis and that it affects the progression of NASH (18,35,36). Given that ferroptosis is critical in regulating the progression of MAFLD, understanding the molecular mechanisms underlying ferroptosis and identifying novel targets to inhibit its occurrence may be an effective approach in the treatment of abnormal ferroptosis-related MAFLD. The present study provides compelling evidence demonstrating that the downregulation of *PLIN5* can inhibit the occurrence of ferroptosis. Mechanistically, PLIN5 may influence the progression of MAFLD and the occurrence of ferroptosis by regulating ATF3 activation. Knockout of *PLIN5* was shown to inhibit expression of the ferroptosis-related genes *ATF3*, *CHOP* and *CHAC1*; in addition, knockdown of *ATF3* could alleviate *PLIN5* overexpression-induced ferroptosis and lipid accumulation in cells. Notably, it has been reported that *ATF1*, *ATF3* and *ATF4* can bind to the *PLIN5* promoter and induce its expression in hepatocytes (37). It may thus be speculated that a positive feedback loop between *PLIN5* and *ATF3* could contribute to the pathogenesis of MAFLD. Moreover, emerging evidence has indicated that phosphorylation of PLIN5 by protein kinase A triggers PLIN5 nuclear translocation and regulates the transcriptional expression of PPARγ coactivator 1-α (38). However, current evidence demonstrates that PLIN5 primarily functions as a transcriptional co-activator or auxiliary factor. It therefore could be hypothesized that PLIN5 may participate in regulating *ATF3* transcriptional expression; however, this requires further validation in luciferase reporter assays and chromatin immunoprecipitation experiments. In addition, a previous study showed that JNK phosphorylation was significantly reduced in a moues model of MAFLD after loss of PLIN5 (39). In another experiment, the JNK inhibitor JM-2 was reported to significantly protect mouse livers from HFD-induced lipid accumulation and apoptosis (40). Therefore, other cell death pathways regulated by PLIN5 may also contribute to the development of MAFLD.

PLINs have been recognized as key proteins involved in lipid accumulation; in particular, the role of PLIN5 in the liver has been extensively studied (9-12). Different models of MAFLD have been established in *PLIN5*$^{-/-}$ mice and have yielded differing results. These conflicting findings may be due to differences in the MAFLD/MASH model and stages of the disease studied. For example, Mass-Sanchez *et al* (41) demonstrated that loss of *PLIN5* protects against worsening of MAFLD by regulating inflammatory signaling, mitochondrial function and lipid metabolism, while in a mouse model of MAFLD-induced hepatocellular carcinoma, *PLIN5* knockout was found to suppress phosphorylated-STAT3 and attenuate the inflammatory response, thereby mitigating severe liver injury. However, in various NASH models, *PLIN5* knockout has been shown to worsen NASH-associated characteristics in mice given a high-fat/high-cholesterol (HFHC) diet, such as lipid accumulation, inflammation and hepatic fibrosis; by contrast, overexpression of *PLIN5* has been shown to ameliorate methionine and choline-deficient (MCD) diet-induced NASH and ferroptosis (42). In a previous study, key points reported regarding the major models were reviewed, as well as the feeding conditions evaluated in each of these models, underpinning the notion that the role of PLIN5 in metabolism appears to be tissue-specific (43). In the current study, PLIN5 was highly expressed in the MAFLD model, and knockout of *PLIN5* could reverse MAFLD. Notably, it was demonstrated that the loss of *PLIN5* could reduce ferroptosis and upregulate the expression of *GPX4*; however, these findings differ from those reported in other studies (42,44), where knockout of *PLIN5* diminished HFHC diet-induced ferroptosis and overexpression of *PLIN5* ameliorated MCD diet-induced NASH and ferroptosis (42). Furthermore, *PLIN5* overexpression has been suggested to ameliorate ferroptosis via the PIR/NF-κB axis in PA-stimulated HL-1 cells (44). In summary, the regulation of ferroptosis by PLIN5 varies in different disease models.

A previous study demonstrated that knocking out *PLIN5* enhances insulin resistance in skeletal muscles by reducing the storage of TGs (45). Moreover, *PLIN5* deletion protects against MAFLD and hepatocellular carcinoma by modulating lipid metabolism and inflammatory responses (41). Gallardo-Montejano *et al* (46) demonstrated that promoting PLIN5 function in BAT was associated with healthy remodeling of subcutaneous white adipose tissue, and an improvement in systemic glucose tolerance, as well as diet-induced hepatic steatosis. These conflicting results may be attributed to the methods used in previous PLIN5-related research related to MAFLD, all of which have focused on systemic rather than local knockout of *PLIN5*. Therefore, crosstalk in the biological effects of PLIN5 in different tissues is possible. Furthermore,

systemic knockout may have off-target metabolic effects. Given that PLIN5 exhibits distinct biological functions across different tissues and cell types, liver-specific knockout mice will be essential to further elucidate the role of PLIN5 in liver metabolism. Furthermore, *ex vivo* liver organoid models, with their operational simplicity, reproducibility and technical accessibility (47,48), may serve as an ideal platform for elucidating how microenvironmental factors mediate the regulatory role of PLIN5 in MAFLD pathogenesis.

ATF3 is a member of the ATF/CREB family of transcription factors (20). Recent research has demonstrated that liver macrophage ATF3 simultaneously inhibits hepatocyte lipogenesis and hepatic stellate cell activation in mice (49). Basak *et al* (50) showed that ATF3 can form a complex with RGS7, which is required for PA-dependent oxidative stress and cell death. *ATF3* has also been identified as a key gene in ferroptosis following spinal cord injury (51), and the soy-derived compound 6j can inhibit liver cancer cell proliferation via ATF3-mediated ferroptosis (52). In addition, evidence has suggested that ATF3 is involved in erastin-induced ferroptosis (53). Therefore, ATF3 may have a critical role in regulating ferroptosis during MASH progression. The present study identified a set of genes associated with ferroptosis, and demonstrated that ATF3 expression was significantly lower in the *PLIN5*$^{-/-}$ HFD group compared with that in the WT HFD group.

The CHOP signaling pathway is also involved in the synergistic interaction between ferroptosis and apoptosis (28), and ATF3/CHOP/BCL2 signaling can control ERS-associated apoptosis (54). CHAC1 is the downstream target of the ATF4/CHOP axis; it possesses γ-glutamyl cyclotransferase activity and also degrades GSH. Notably, depletion of GSH is a crucial factor in apoptosis initiation and execution (55). Endoplasmic reticulum-mediated apoptosis is also activated via the ATF4/CHOP/CHAC1 cascade (56). Given these findings, it may be hypothesized that ATF3 is the interacting target of PLIN5, which affects ferroptosis, oxidative damage and lipid accumulation. The present study revealed that the expression levels of CHOP and CHAC1 were reduced in *PLIN5*$^{-/-}$ HFD mice compared with those in WT HFD mice. Furthermore, knockdown of *ATF3* alleviated lipid accumulation and ferroptosis induced by *PLIN5* overexpression. Emerging evidence has revealed that PLIN5 not only functions as an LD-coating protein localized on LDs, but that its phosphorylated form can also translocate into the nucleus to participate in transcriptional regulation. This dual functionality markedly enhances the complexity of the reciprocal regulatory network between PLIN5 and transcription factor ATF3, warranting further mechanistic investigation (34,57). Owing to limitations in clinical specimen availability, the current study was unable to examine the association between PLIN5 and ferroptosis-related proteins (including ATF3, CHOP and CHAC1) in human fatty liver tissues. Notably, a previous study reported that the protein expression of PLIN5 was markedly elevated in the severely steatotic livers of included patients (58). Moreover, ATF3 has been reported to be highly expressed in the livers of Zucker diabetic fatty rats and in human participants with MAFLD and/or type 2 diabetes (59).

As indicated in the current guidelines (AASLD (60), very few drugs are recommended for MAFLD treatment. To date, only vitamin E and the PPARγ ligand pioglitazone have been endorsed for limited patients by the European-and American Association for the Study of the Liver (61). Given the central roles of PLIN5 in LD stabilization and ATF3 in hepatic stress response, as demonstrated by the present study, pharmacological inhibition of these targets represents a mechanistically rational strategy for MAFLD intervention. Patients with hypercholesterolemia routinely receive statins, HMG-CoA reductase inhibitors that block *de novo* cholesterol biosynthesis. Previous studies have demonstrated that statins reduce PLIN5 levels in murine/human hepatocytes, concomitant with decreased TGs and LD quantity. This effect is mediated by an atypical sterol-regulatory sequence in the *PLIN5* promoter, where *SREBP2* binding confers statin responsiveness (62,63). Crucially, partial *PLIN5* knockdown can mimic statin-induced TG reduction, while *PLIN5* overexpression reverses it (62). Thus, combining PLIN5 inhibitors with statins may yield synergistic anti-MAFLD effects. Notably, Yu *et al* (64) proposed targeting ATF3 with engineered peptide inhibitors, providing a compelling rationale for developing ATF3-targeted therapies against MAFLD.

In conclusion, the present study identified a link from PLIN5 to ferroptosis and MAFLD via the ATF3/CHOP/CHAC1 axis, thereby providing insights into the mechanism of ferroptosis in MAFLD progression. Knocking down *PLIN5* may target the ATF3/CHOP/CHAC1 signaling axis, which attenuates ferroptosis in liver cells, eventually alleviating MAFLD. The present findings may lay the foundation for a promising therapeutic strategy in the treatment of MAFLD.

Acknowledgements

Not applicable.

Funding

The present study was supported by research grants from the National Natural Science Foundation of China (grant no. 31471330), the Henan Provincial Medical Science and Technology Tackling Program Co-construction Project (grant nos. LHGJ20210483 and LHGJ20220557), the Zhengzhou University Discipline Key Special Project (grant no. XKZDQY202001), the Henan Province Foreign Intelligence Introduction Program (grant no. GZS2022008), Science and Technology Projects (grant no. 242102310228), the Zhengzhou Science and Technology Benefit to the People Project (grant no. 2022KJHM0020) and the Key Research and Development Projects of Henan Province (grant no. 241111210500).

Availability of data and materials

The raw RNA-seq data generated in the present study may be found in the NCBI Sequence Read Archive under accession number PRJNA1295086 or at the following URL: https://www.ncbi.nlm.nih.gov/bioproject/PRJNA1295086/. The raw single-cell RNA-seq data generated in the present study may be found in the China National Center for Bioinformation under accession number CRA018673 or at the following URL: https://ngdc.cncb.ac.cn/gsa/search?searchTerm=CRA018673. The

other data generated in the present study may be requested from the corresponding author.

Authors' contributions

Experiments were performed by YT, YL, XW and XY, with the help of LD, WC and YX. Experiments were designed by YL and XW, with the help of PZ and YW. LD, XZ and LL managed animals and performed animal experiments. XW, XY and YL analyzed the data. YL wrote the paper, with assistance from YT, XW and XY in editing and revisions. PZ and YT supervised the work, and confirm the authenticity of all the raw data. All authors made significant contributions to the article, and read and approved the final manuscript.

Ethics approval and consent to participate

The animal study was approved by the Ethics Committee of Zhengzhou University (approval no. KY2023006). The study was performed in accordance with Institutional Animal Care and Use Committee guidelines; all procedures were carried out in accordance with institutional guidelines.

Patient consent for publication

Not applicable.

Competing interests

The authors declare that they have no competing interests.

References

1. Rinella ME, Neuschwander-Tetri BA, Siddiqui MS, Abdelmalek MF, Caldwell S, Barb D, Kleiner DE and Loomba R: AASLD Practice Guidance on the clinical assessment and management of nonalcoholic fatty liver disease. Hepatology 77: 1797-1835, 2023.
2. Yip TCF, Vilar-Gomez E, Petta S, Yilmaz Y, Wong GL, Adams LA, de Lédinghen V, Sookoian S and Wong VW: Geographical similarity and differences in the burden and genetic predisposition of NAFLD. Hepatology 77: 1404-1427, 2023.
3. Syed-Abdul MM: Lipid metabolism in Metabolic-associated steatotic liver disease (MASLD). Metabolites 14: 12, 2024.
4. Guo X, Yin X, Liu Z and Wang J: Non-alcoholic fatty liver disease (NAFLD) pathogenesis and natural products for prevention and treatment. Int J Mol Sci 23: 15489, 2022.
5. Petta S, Targher G, Romeo S, Pajvani UB, Zheng MH, Aghemo A and Valenti LVC: The first MASH drug therapy on the horizon: Current perspectives of resmetirom. Liver Int 44: 1526-1536, 2024.
6. Herker E, Vieyres G, Beller M, Krahmer N and Bohnert M: Lipid droplet contact sites in health and disease. Trends Cell Biol 31: 345-358, 2021.
7. Gluchowski NL, Becuwe M, Walther TC and Farese RV Jr: Lipid droplets and liver disease: From basic biology to clinical implications. Nat Rev Gastroenterol Hepatol 14: 343-355, 2017.
8. Najt CP, Khan SA, Heden TD, Witthuhn BA, Perez M, Heier JL, Mead LE, Franklin MP, Karanja KK, Graham MJ, *et al*: Lipid Droplet-derived monounsaturated fatty acids traffic via PLIN5 to allosterically activate SIRT1. Mol Cell 77: 810-824.e8, 2020.
9. Mason RR and Watt MJ: Unraveling the roles of PLIN5: Linking cell biology to physiology. Trends Endocrinol Metab 26: 144-152, 2015.
10. Asimakopoulou A, Engel KM, Gassler N, Bracht T, Sitek B, Buhl EM, Kalampoka S, Pinoé-Schmidt M, van Helden J, Schiller J and Weiskirchen R: Deletion of perilipin 5 protects against hepatic injury in nonalcoholic fatty liver disease via missing inflammasome activation. Cells 9: 1346, 2020.
11. Ma Y, Yin X, Qin Z, Ke X, Mi Y, Zheng P and Tang Y: Role of Plin5 deficiency in progression of Non-alcoholic fatty liver disease induced by a High-fat diet in mice. J Comp Pathol 189: 88-97, 2021.
12. Yin X, Dong L, Wang X, Qin Z, Ma Y, Ke X, Li Y, Wang Q, Mi Y, Lyu Q, *et al*: Perilipin 5 regulates hepatic stellate cell activation and high-fat diet-induced non-alcoholic fatty liver disease. Animal Model Exp Med 7: 166-178, 2024.
13. Jiang X, Stockwell BR and Conrad M: Ferroptosis: Mechanisms, biology and role in disease. Nat Rev Mol Cell Biol 22: 266-282, 2021.
14. Wu J, Wang Y, Jiang R, Xue R, Yin X, Wu M and Meng Q: Ferroptosis in liver disease: New insights into disease mechanisms. Cell Death Discov 7: 276, 2021.
15. Zhou X, Fu Y, Liu W, Mu Y, Zhang H, Chen J and Liu P: Ferroptosis in chronic liver diseases: Opportunities and challenges. Front Mol Biosci 9: 928321, 2022.
16. Wang S, Liu Z, Geng J, Li L and Feng X: An overview of ferroptosis in Non-alcoholic fatty liver disease. Biomed Pharmacother 153: 113374, 2022.
17. Zhang H, Axinbai M, Zhao Y, Wei J, Qu T, Kong J, He Y and Zhang L: Bioinformatics analysis of Ferroptosis-related genes and immune cell infiltration in non-alcoholic fatty liver disease. Eur J Med Res 28: 605, 2023.
18. Yin X, Mi Y, Wang X, Li Y, Zhu X, Bukhari I, Wang Q, Zheng P, Xue X and Tang Y: Exploration and validation of Ferroptosis-associated genes in ADAR1 Deletion-induced NAFLD through RNA-seq analysis. Int Immunopharmacol 134: 112177, 2024.
19. Fu D, Wang C, Yu L and Yu R: Induction of ferroptosis by ATF3 elevation alleviates cisplatin resistance in gastric cancer by restraining Nrf2/Keap1/xCT signaling. Cell Mol Biol Lett 26: 26, 2021.
20. Zhao X, Wang Z, Wu G, Yin L, Xu L, Wang N and Peng J: Apigenin-7-glucoside-loaded nanoparticle alleviates intestinal ischemia-reperfusion by ATF3/SLC7A11-mediated ferroptosis. J Control Release 366: 182-193, 2024.
21. Inaba Y, Hashiuchi E, Watanabe H, Kimura K, Oshima Y, Tsuchiya K, Murai S, Takahashi C, Matsumoto M, Kitajima S, *et al*: The transcription factor ATF3 switches cell death from apoptosis to necroptosis in hepatic steatosis in male mice. Nat Commun 14: 167, 2023.
22. National Research Council (US) Institute for Laboratory Animal Research: The Development of Science-based Guidelines for Laboratory Animal Care: Proceedings of the November 2003 International Workshop. National Academies Press, Washington DC, 2004.
23. Hu Y, He W, Huang Y, Xiang H, Guo J, Che Y, Cheng X, Hu F, Hu M, Ma T, *et al*: Fatty acid synthase-suppressor screening identifies sorting Nexin 8 as a therapeutic target for NAFLD. Hepatology 74: 2508-2525, 2021.
24. Ren Y, Mao X, Xu H, Dang Q, Weng S, Zhang Y, Chen S, Liu S, Ba Y, Zhou Z, *et al*: Ferroptosis and EMT: Key targets for combating cancer progression and therapy resistance. Cell Mol Life Sci 80: 263, 2023.
25. Chen GH, Song CC, Pantopoulos K, Wei XL, Zheng H and Luo Z: Mitochondrial oxidative stress mediated Fe-induced ferroptosis via the NRF2-ARE pathway. Free Radic Biol Med 180: 95-107, 2022.
26. Asghari S, Hamedi-Shahraki S and Amirkhizi F: Systemic redox imbalance in patients with nonalcoholic fatty liver disease. Eur J Clin Invest 50: e13211, 2020.
27. Bathish B, Robertson H, Dillon JF, Dinkova-Kostova AT and Hayes JD: Nonalcoholic steatohepatitis and mechanisms by which it is ameliorated by activation of the CNC-bZIP transcription factor Nrf2. Free Radic Biol Med 188: 221-261, 2022.
28. Hong SH, Lee DH, Lee YS, Jo MJ, Jeong YA, Kwon WT, Choudry HA, Bartlett DL and Lee YJ: Molecular crosstalk between ferroptosis and apoptosis: Emerging role of ER stress-induced p53-independent PUMA expression. Oncotarget 8: 115164-115178, 2017.
29. Mungrue IN, Pagnon J, Kohannim O, Gargalovic PS and Lusis AJ: CHAC1/MGC4504 is a novel proapoptotic component of the unfolded protein response, downstream of the ATF4-ATF3-CHOP cascade. J Immunol 182: 466-476, 2009.
30. Stockwell BR: Ferroptosis turns 10: Emerging mechanisms, physiological functions, and therapeutic applications. Cell 185: 2401-2421, 2022.
31. Golabi P, Paik JM, AlQahtani S, Younossi Y, Tuncer G and Younossi ZM: Burden of non-alcoholic fatty liver disease in Asia, the Middle East and North Africa: Data from global burden of disease 2009-2019. J Hepatol 75: 795-809, 2021.

32. Li, J, Wang T, Liu P, Yang F, Wang X, Zheng W and Sun W: Hesperetin ameliorates hepatic oxidative stress and inflammation via the PI3K/AKT-Nrf2-ARE pathway in oleic acid-induced HepG2 cells and a rat model of high-fat diet-induced NAFLD. Food Funct 12: 3898-3918, 2021.
33. Tong J, Lan X, Zhang, Z, Liu Y, Sun D, Wang X, Ou-Yang SX, Zhuang CL, Shen FM, Wang P and Li DJ: Ferroptosis inhibitor liproxstatin-1 alleviates metabolic dysfunction-associated fatty liver disease in mice: Potential involvement of PANoptosis. Acta Pharmacol Sin 44: 1014-1028, 2023.
34. Chen X, Li J, Kang R, Klionsky DJ and Tang D: Ferroptosis: Machinery and regulation. Autophagy 17: 2054-2081, 2021.
35. Tsurusaki S, Tsuchiya Y, Koumura T, Nakasone M, Sakamoto T, Matsuoka M, Imai H, Yuet-Yin Kok C, Okochi H, Nakano H, *et al*: Hepatic ferroptosis plays an important role as the trigger for initiating inflammation in nonalcoholic steatohepatitis. Cell Death Dis 10: 449, 2019.
36. Guan Q, Wang Z, Hu K, Cao J, Dong Y and Chen Y: Melatonin ameliorates hepatic ferroptosis in NAFLD by inhibiting ER stress via the MT2/cAMP/PKA/IRE1 signaling pathway. Int J Biol Sci 19: 3937-3950, 2023.
37. Tan Y, Jin Y, Wang Q, Huang J, Wu X and Ren Z: Perilipin 5 Protects against cellular oxidative stress by enhancing mitochondrial function in HepG2 cells. Cells 8: 1241, 2019.
38. Gallardo-Montejano VI, Saxena G, Kusminski CM, Yang C, McAfee JL, Hahner L, Hoch K, Dubinsky W, Narkar VA and Bickel PE: Nuclear Perilipin 5 integrates lipid droplet lipolysis with PGC-1α/SIRT1-dependent transcriptional regulation of mitochondrial function. Nat Commun 7: 12723, 2016.
39. Fang Z, Xu H, Duan J, Ruan B, Liu J, Song P, Ding J, Xu C, Li Z, Dou K and Wang L: Short-term tamoxifen administration improves hepatic steatosis and glucose intolerance through JNK/MAPK in mice. Signal Transduct Target Ther 8: 94, 2023.
40. Jin L, Wang M, Yang B, Ye L, Zhu W, Zhang Q, Lou S, Zhang Y, Luo W and Liang G: A small-molecule JNK inhibitor JM-2 attenuates high-fat diet-induced non-alcoholic fatty liver disease in mice. Int Immunopharmacol 115: 109587, 2023.
41. Mass-Sanchez PB, Krizanac M, Štancl P, Leopold M, Engel KM, Buhl EM, van Helden J, Gassler N, Schiller J, Karlić R, *et al*: Perilipin 5 deletion protects against nonalcoholic fatty liver disease and hepatocellular carcinoma by modulating lipid metabolism and inflammatory responses. Cell Death Discov 10: 94, 2024.
42. Xu X, Qiu J, Li X, Chen J, Li Y, Huang X, Zang S, Ma X and Liu J: Perilipin5 protects against Non-alcoholic steatohepatitis by increasing 11-Dodecenoic acid and inhibiting the occurrence of ferroptosis. Nutr Metab (Lond) 20: 29, 2023.
43. Mass Sanchez PB, Krizanac M, Weiskirchen R and Asimakopoulos A: Understanding the role of perilipin 5 in Non-alcoholic fatty liver disease and its role in hepatocellular carcinoma: A review of novel insights. Int J Mol Sci 22: 5284, 2021.
44. Shen X, Zhang J, Zhou Z and Yu R: PLIN5 suppresses lipotoxicity and ferroptosis in cardiomyocyte via modulating PIR/NF-κB Axis. Int Heart J 65: 537-547, 2024.
45. Mason RR, Mokhtar R, Matzaris M, Selathurai A, Kowalski GM, Mokbel N, Meikle PJ, Bruce CR and Watt MJ: PLIN5 deletion remodels intracellular lipid composition and causes insulin resistance in muscle. Mol Metab 3: 652-663, 2014.
46. Gallardo-Montejano VI, Yang C, Hahner L, McAfee JL, Johnson JA, Holland WL, Fernandez-Valdivia R and Bickel PE: Perilipin 5 links mitochondrial uncoupled respiration in brown fat to healthy white fat remodeling and systemic glucose tolerance. Nat Commun 12: 3320, 2021.
47. Navik U, Singh SK, Khurana A and Weiskirchen R: Revolutionizing liver fibrosis research: The promise of 3D organoid models in understanding and treating chronic liver disease. Expert Rev Gastroenterol Hepatol 19: 105-110, 2025.
48. Liu Y, Gilchrist AE, Johansson PK, Guan Y, Deras JD, Liu YC, Ceva S, Huang MS, Navarro RS, Enejder A, *et al*: Engineered hydrogels for organoid models of human nonalcoholic fatty liver disease. Adv Sci (Weinh) 12: e17332, 2025.
49. Hu S, Li R, Gong D, Hu P, Xu J, Ai Y, Zhao X, Hu C, Xu M, Liu C, *et al*: Atf3-mediated metabolic reprogramming in hepatic macrophage orchestrates metabolic dysfunction-associated steatohepatitis. Sci Adv 10: eado3141, 2024.
50. Basak M, Das K, Mahata T, Sengar AS, Verma SK, Biswas S, Bhadra K, Stewart A and Maity B: RGS7-ATF3-Tip60 complex promotes hepatic steatosis and fibrosis by directly inducing TNFα. Antioxid Redox Signal 38: 137-159, 2023.
51. Kang Y, Li Q, Zhu R, Li S, Xu X, Shi X and Yin Z: Identification of Ferroptotic genes in spinal cord injury at different time points: Bioinformatics and experimental validation. Mol Neurobiol 59: 5766-5784, 2022.
52. Tian K, Wei J, Wang R, Wei M, Hou F and Wu L: Sophoridine derivative 6j inhibits liver cancer cell proliferation via ATF3 mediated ferroptosis. Cell Death Discov 9: 296, 2023.
53. Wang L, Liu Y, Du T, Yang H, Lei L, Guo M, Ding HF, Zhang J, Wang H, Chen X and Yan C: ATF3 promotes erastin-induced ferroptosis by suppressing system Xc. Cell Death Differ 27: 662-675, 2020.
54. Alosaimi M, Abd-Elhakim YM, Mohamed AA, Metwally MMM, Khamis T, Alansari WS, Eskandrani AA, Essawi WM, Awad MM, El-Shaer RAA, *et al*: Green synthesized zinc oxide nanoparticles attenuate acrylamide-induced cardiac injury via controlling endoplasmic reticulum stress-associated apoptosis through ATF3/CHOP/BCL2 signaling in rats. Biol Trace Elem Res 202: 2657-2671, 2024.
55. Crawford RR, Prescott ET, Sylvester CF, Higdon AN, Shan J, Kilberg MS and Mungrue IN: Human CHAC1 protein degrades glutathione, and mRNA induction is regulated by the transcription factors ATF4 and ATF3 and a bipartite ATF/CRE regulatory element. J Biol Chem 290: 15878-15891, 2015.
56. Wang X, He MJ, Chen XJ, Bai YT and Zhou G: Glaucocalyxin A impairs tumor growth via amplification of the ATF4/CHOP/CHAC1 cascade in human oral squamous cell carcinoma. J Ethnopharmacol 290: 115100, 2022.
57. Drummer C IVth, Saaoud F, Jhala NC, Cueto R, Sun Y, Xu K, Shao Y, Lu Y, Shen H, Yang L, *et al*: Caspase-11 promotes high-fat diet-induced NAFLD by increasing glycolysis, OXPHOS, and pyroptosis in macrophages. Front Immunol 14: 1113883, 2023.
58. Ma SY, Sun KS, Zhang M, Zhou X, Zheng XH, Tian SY, Liu YS, Chen L, Gao X, Ye J, *et al*: Disruption of Plin5 degradation by CMA causes lipid homeostasis imbalance in NAFLD. Liver Int 40: 2427-2438, 2020.
59. Kim JY, Park KJ, Hwang JY, Kim GH, Lee D, Lee YJ, Song EH, Yoo MG, Kim BJ, Suh YH, *et al*: Activating transcription factor 3 is a target molecule linking hepatic steatosis to impaired glucose homeostasis. J Hepatol 67: 349-359, 2017.
60. Cusi K, Isaacs S, Barb D, Basu R, Caprio S, Garvey WT, Kashyap S, Mechanick JI, Mouzaki M, Nadolsky K, *et al*: American association of clinical endocrinology clinical practice guideline for the diagnosis and management of nonalcoholic fatty liver disease in primary care and endocrinology clinical settings: Co-sponsored by the American association for the study of liver diseases (AASLD). Endocr Pract 28: 528-562, 2022.
61. Paternostro R and Trauner M: Current treatment of non-alcoholic fatty liver disease. J Intern Med 292: 190-204, 2022.
62. Langhi C, Marquart TJ, Allen RM and Baldán A: Perilipin-5 is regulated by statins and controls triglyceride contents in the hepatocyte. J Hepatol 61: 358-365, 2014.
63. Gao X, Nan Y, Zhao Y, Yuan Y, Ren B and Sun C: Atorvastatin reduces lipid accumulation in the liver by activating protein kinase A-mediated phosphorylation of perilipin 5. Biochim Biophys Acta Mol Cell Biol Lipids 1862: 1512-1519, 2017.
64. Yu M, Tang TMS, Ghamsari L, Yuen G, Scuoppo C, Rotolo JA, Kappel BJ and Mason JM: Exponential Combination of a and e/g intracellular peptide libraries identifies a selective ATF3 inhibitor. ACS Chem Biol 19: 753-762, 2024.